Sustainable Energy & Fuels

Plasmonic Interfacial Evaporator for High-Efficiency Solar Vapor Generation

Journal:	*Sustainable Energy & Fuels*
Manuscript ID	SE-ART-08-2018-000402.R1
Article Type:	Paper
Date Submitted by the Author:	28-Sep-2018
Complete List of Authors:	Tao, Fujun; Shanghai Maritime University Zhang, Yuliang; Shanghai Maritime University, Yin, Kuan; Shanghai Maritime University Cao, Shengjia; Shanghai Maritime University Chang, Xueting; Shanghai Maritime University Lei, Yanhua; Shanghai Maritime University Wang, Dongsheng; Shanghai Maritime University Fan, Runhua; Shanghai Maritime University, College of Ocean Science and Engineering dong, lihua; Shanghai Maritime University, Institute of Marine Materials Science and Engineering yin, yansheng; Shanghai Maritime University, Institute of Marine Materials Science and Engineering Chen, Xiaobo; University of Missouri - Kansas City, Chemistry

Journal Name

ARTICLE

Plasmonic Interfacial Evaporator for High-Efficiency Solar Vapor Generation

X Received 00th January 20xx,
Accepted 00th January 20xx

DOI: 10.1039/x0xx00000x

www.rsc.org/

Fujun Tao,[a] Yuliang Zhang,*[a] Kuan Yin,[a] Shengjia Cao,[a] Xueting Chang,[a] Yanhua Lei,[a] Dongsheng Wang,[a] Runhua Fan,[a] Lihua Dong,[a] Yansheng Yin,[a] and Xiaobo Chen*[b]

The increasing energy and environmental concerns have spurred enormous research interests on various renewable energy and sustainable environmental solutions. Photothermal conversion for interfacial solar vapor generation is a promising, green energy technology and efficient route for desalination and purification of seawater, i.e. for those parts where freshwater shortage is a severe concern and clean energy is not available. Eco-friendly, highly-efficient and low-cost interfacial evaporators are highly desirable for the practical and wide application of this technology. In this work, we have demonstrated a novel interfacial evaporator employing Cu_9S_5 nanonets with heterogeneous hexagonalholes as photothermal conversion material and microporous poly(vinylidene fluoride) membrane (PVDFM) as the supporting material. The Cu_9S_5/PVDFM evaporator displays a broadband (from 250 to 2000 nm) and large (~91.7%) solar absorptance. The porous structures of Cu_9S_5 nanonets and PVDFM facilitate the water transportation, and the large optical absorption of Cu_9S_5/PVDFM converts most of the solar energy to thermal energy, producing water vapor with high efficiency. The Cu_9S_5/PVDFM evaporator has exhibited solar vapor generation efficiencies of 80.2±0.6% and 91.5±1.1% under one-sun and four-sun irradiation, respectively, among the best copper sulphide-based solar evaporators reported so far. This Cu_9S_5/PVDFM evaporator is reusable, flexible, highly efficient, easy to prepare, easy to scale up, and controllable for tailoring, showing a promising future for interfacial solar vapor generation.

Introduction

The daily increasing clean energy and environmental needs have spurred enormous research interests around the world in developing various renewable energy and environmental solutions. Efficient utilization of solar energy in various forms have provided some good promise and also expanded our visions on the means of using solar energy, which is clean and free of the concerns of depletion. Among the various possible usage of solar energy,[1-6] photothermal conversion is one of the most promising and efficient approaches that can efficiently produce hot water and distilled clean water with a high efficiency. Today, because of the increasingly population growth, expanded industrial and environmental contamination concerns, many parts of the word are suffering serious freshwater shortage problem.[7-8] Interfacial solar vapor generation is becoming very attractive and efficient for seawater desalination, compared to the conventional route of heating up bulk water to generate steam/vapor. The interfacial solar vapor generatotion can localize the solar energy at the interface where vapor is generated and decrease the heat loss in the water evaporation process, enhancing the solar vapor generation efficiency and rate under low intensity of solar irradiation,[9] because it does not need to heat the bulk water beneath the air-water interface that does not take part in generating vapor but also consumes the absorbed solar energy.

The structures of the interfacial evaporators are critical to achieve high efficiency.[10-14] Many types have been reported, such as integrated structure,[10-11] bi-layer structure[12-13] and multi-layer structure.[14] Photothermal conversion materials and supporting materials play key roles in those structures. Ideal photothermal conversion materials should have a large and wide absorption in the solar spectrum and be able to convert the absorbed solar energy into heat efficiently, and ideal supporting materials should have low density, low thermal conductivity, high porosity and excellent thermal stability. Common photothermal conversion materials include carbon-based materials (e.g., exfoliated graphite,[15] carbon nanotube,[16] graphite powder,[17] graphene,[18] graphene oxide,[19] reduced graphene oxide[12,20]), plasmonic-metals (e.g., Au,[21-26] Ag,[27-28] Al,[29] Pd[30]), plasmonic-ceramics (e.g., TiN,[31] Ti_3C_2[32,33]), plasmonic-semiconductors (e.g., $Cu_{2-x}S$,[34-38] $Cu_{2-x}Se$,[39] $Cu_{2-x}Te$,[40] $W_{18}O_{49}$,[41,42] WO_{3-x}[43]), and other light-harvesting materials (e.g., Ti_2O_3,[44] MoS_2,[45,46] carbonized mushroom[47]). And the supporting materials include paper-,[24,25,48] wood-,[30,49,50] foam-,[15] membrane-,[10,12,17] gel-,[51-53] and gauze-based materials.[54] Although higher efficiencies are becoming feasible upon continuous developments in this field, ideal system needs not

[a] College of Ocean Science and Engineering, Shanghai Maritime University, Shanghai 201306, P.R. China, E-mail: ylzhang@shmtu.edu.cn
[b] Department of Chemistry, University of Missouri-Kansas City, Kansas City, MO 64110, USA,E-mail: chenxiaobo@umkc.edu

only high efficiency, but also an eco-friendly, efficient, cost-effective interfacial solar evaporator. The components insides should be inexpensive, no toxicity, and have long lifetime.

Gold nanoparticles have been investigated extensively in solar-energy-harvesting field due to their good capability in absorbing effectively sunlight in a wide wavelength range from the localized surface plasmon resonance (LSPRs). For instance, Bae et al.[21] reported a black gold membrane for solar vapor generation with water evaporation efficiency of ~57% under 20 sun. Naik et al.[22] reported a plasmonic Au aerogel for water evaporation with a steam generation efficiency of ~76.3% under 808 nm laser with the power density of 51 kW m^{-2}. Zhu et al.[23] reported an Au/nanoporous alumina template composite for solar vapor generation with a water evaporation efficiency of ~65% under 4 sun. Deng et al.[24] reported an airlaid-paper-based Au nanopariticle film for solar vapor generation with a water evaporation efficiency of ~77.8% under 4.5 sun. He et al.[25] reported an Au/filter paper composite for solar steam generation with an efficiency value of ~85% under 10 sun. He et al.[26] reported an Au/poly(*p*-phenylene benzobisoxazole) nanofiber composite for solar steam generation with an efficiency value of ~83% under 1 sun. Despite of the gradual increase in the solar vapor generation efficiency of plasmonic-Au based evaporators, one major demerit is that the gold nanoparticles are easily aggregated and fused together at high temperature resulting from long-time of solar irradiation, causing the degradation of the water evaporation performance over time. The other major obstacle for gold-based evaporators is the high cost, which limits their wide, large-scale production, even if the efficiency can be very high.

Eying to solve the high cost problem that the gold-based evaporators have, other solar absorbing materials are sought with LSPRs as well with some transition metal semiconducting materials.[31,32,55,56] For example, various solid phases of $Cu_{2-x}S$ ($0 \leqslant X \leqslant 1$) have been reported, ranging from copper-rich Cu_2S to copper-poor CuS (e.g. chalcocite Cu_2S,[57] djuleite $Cu_{1.96}S$,[58] digenite $Cu_{1.8}S$,[36] anilite $Cu_{1.75}S$,[38] and covellite CuS[34]) and with various nanostructures and morphologies (e.g., nanorods,[35] nanoplates,[59] nanonets,[36] nanowires,[60] nanoflowers,[34] nanotubes,[61] nanovesicles[62]). Compared with other plasmonic materials (e.g., Au,[21-26] Ag[27-28]), copper sulphide semiconductors materials display low cost, low cytotoxicity, and outstanding light-stability features, and have been regarded as one of the most promising green and sustainable energy materials for solar vapor generation,[13,34,35,63] etc. For example, Wang et al.[63] reported an evaporator composed of CuS nanoparticles and polyethylene hybrid membrane for solar vapor generation with a water evaporation efficiency of ~63.5% under 1 sun. In our previous work,[34] an evaporator comprising CuS nanoflowers and semipermeable collodion membrane (SCM) had a water evaporation efficiency of ~68.6% under 1 sun. Wang et al.[13] reported bi-layer structural evaporators composed of Cu_xS and mixed cellulose ester (MCE) film for solar vapor generation, e.g., octahedral Cu_9S_5 nanocrystal/MCE composite with an evaporation efficiency of ~60.1%, and granular CuS nanocrystal/MCE composite with an appreciable efficiency ~80% under 1 sun, respectively. The photothermal conversion material of Cu_xS nanoparticle was filtered on the surface of MCE film by a vacuum filtration method to form a bi-layer structural evaporation system.[13] Although high water evaporation efficiency has been demonstrated, the Cu_xS nanoparticle located at the top layer could detach from the bottom layer (the MCE film) after a long-time solar irradiation or/and high-usage levels due to the low-adhesion between the top and bottom layers. Besides, the effect of natural water evaporation is very important and should be subtracted when calculating the water evaporation efficiency under solar irradiation, which was, however, neglected in some previous works.[13,34,63] In view of this, the actual evaporation efficiencies of the interfacial evaporators in the above-mentioned works are lower than what they reported. Therefore, it is essential to prepare an evaporator with high solar water evaporation efficiency and excellent reusability for solar vapor generation.

In this work, we report an integrative membraneous interfacial evaporator comprising Cu_9S_5 nanonets with heterogeneous hexagonal holes as light-harvesting material and PVDFM as supporting material for solar vapor generation. PVDFM has already been previously reported as outstanding supporting material to prepare several desalination devices due to its major benefits of low-density, microporous structure, and good hydrophilicity.[10,27,32,64,65] Here, our Cu_9S_5/PVDFM device has several advantages: 1) Broadband (250-2000 nm) and large solar absorptance (~91.7%). 2) Unique porous structures. Both Cu_9S_5 and PVDFM are porous, i.e., the Cu_9S_5 nanonets have a unique heterogeneous hexagonal hole structure, and the PVDFM has a microporous structure. These unique porous structures can jointly facilitate the water transportation. 3) Excellent physical compatibility. Cu_9S_5 is distributed uniformly in the integrative membraneous Cu_9S_5/PVDFM composite, including the interior or/and the surface of PVDFM. 4) Easy fabrication process. The preparation procedure of Cu_9S_5/PVDFM composite is easy and simple. 5) Low cost. The production cost of Cu_9S_5/PVDFM is low. 6) excellent durability and reusability. This Cu_9S_5/PVDFM has been reused over 20 cycles without descrease of water evaporation performance, showing an outstanding reusability. Impressively, high water evaporation efficiencies of 80.2±0.6% and 91.5±1.1% were obtained under 1 sun and 4 sun irradiation, respectively. Therefore, it has showed a great potential for solar vapor generation, and may be beneficial for other solar-heating applications such as sterilization, power generation, and solar distillation.

Results and discussion

The Cu_9S_5 nanonets showed a wide optical-absorption over the visible wavelength region of 300-700 nm due to the bandgap (~1.5 eV) absorption and an increased light absorption in the NIR region due to the LSPRs of free carrier in Cu_9S_5 nanonets as shown in Figure 1A. It is well known that ideal solar-harvesting material should have an electromagnetic radiation absorption as much as possible over the full solar spectrum wavelength

range (300 nm-2500 nm), in which the visible wavelength region is from 400 to 700 nm wavelength, occupying ~45% of the solar energy, and the IR wavelength region is from 700-2500 nm, accounting for ~52% of solar energy.[44,53] The inset of Figure 1B showed the photo of the Cu_9S_5/PVDFM disk with a diameter of 33.5 mm. To confirm its light-absorption capability, the UV-vis-NIR absorption spectrum was measured, as calculated from its transmittance and diffuse reflectance spectra. The pure PVDFM was white and opaque with near zero transmittance, high (~95%) diffuse reflectance and very low (5%) absorption in the entire solar spectrum region, consistent with previous reports.[10,32,64] While the Cu_9S_5/PVDFM was black and had near zero transmission, low reflection (<9%), and high (>91%) absorption, as shown in the transmission / reflection / absorption spectra in Figure 1B. Specifically, it can absorb ~91.4% of UV, ~92.4% of visible, and ~90.9% of infrared solar irradiation energy with a total solar absorptance of ~91.7% in the 250-2000 nm wavelength region, as shown in Table 1.

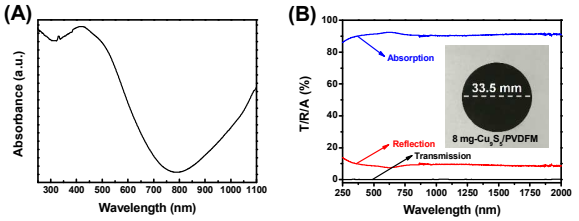

Figure 1. (A) UV-vis-NIR absorption spectrum of as-obtained Cu_9S_5 nanonets; (B) UV-vis-NIR transmission/reflection/absorption spectra and digital photograph (inset of figure B) of 8 mg-Cu_9S_5/PVDFM.

Table 1. Solar absorption of Cu_9S_5/PVDFM in different solar spectrum region.

Sample	UV (250-400 nm)	Visible (400-760 nm)	Infrared (760-2000nm)	Solar absorptance
AM 1.5	~7%	~50%	~39.7%	~91.7%
Cu_9S_5/PVDFM	~6.4%	~46.2%	~36.1%	

Furthermore, the structure and morphology of Cu_9S_5/PVDFM were analyzed by a field-emission scanning electron microscope and a leica microscope, respectively. Unique porous nanonet structure of Cu_9S_5 with heterogeneous hexagonal holes were seen in Figures 2A-B, which could facilitate effectively the water from the bulk water to the water-air interface where water vapor generates. Meanwhile, the surface morphology of Cu_9S_5/PVDFM was poly-porous structure with an average open size of 200 nm as shown in Figures 2C and 2D. As shown in Figure 2E, the initial surface contact angle was 75±1° for the bottom side, showing a hydrophilicity which could facilitate the transport of the water from the bulk beneath the film to the water-air interface. The contact angle for the upper side was 125±1° (see Figure 2F), which demonstrated a good hydrophobicity that could benefit for localizing heat around the water drops on the film. The unique hydrophilic-hydrophobic characteristics of the film was easily recognized in that the bottom side (i.e., hydrophilic side) was smooth and the upper side (i.e., hydrophobic side) was rough, in accordance with the previous report.[10]

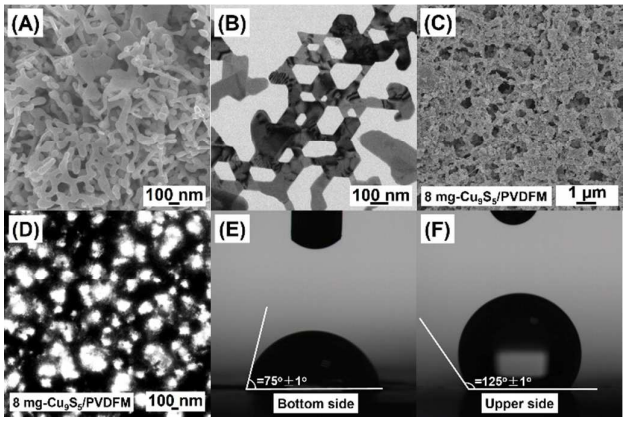

Figure 2. (A) SEM image and (B) TEM of Cu_9S_5 nanonets with heterogeneous hexagonal holes; SEM image (C) and optical microscope image (D) of 8 mg-Cu_9S_5/PVDFM; The surface contact angles of the bottom side (E) and upper side (F) of 8 mg-Cu_9S_5/PVDFM.

To study the solar vapor generation performance, water evaporation tests were performed on a series of Cu_9S_5/PVDFMs with different amounts of Cu_9S_5 nanonets added (i.e., 1, 2, 4, 8 and 12 mg per disk). Figure 3A showed the weight changes of pure water covered with Cu_9S_5/PVDFMs under 1 sun irradiation. For comparison, the weight changes of pure water and pure water covered with pure PVDFM under 1 sun were also tested. Here, it is important to note that the weight change of pure water under dark environment was also tested, and subtracted from all the measured weight changes under solar irradiation to eliminate the effect of natural water evaporation. The average weight changes (i.e., the water evaporated weights) increased from 0.275, 0.396, 0.526, 0.586 and 0.580 kg m^{-2} when the amount of Cu_9S_5 nanonets increased from 1 mg to 12 mg. The increased contents of Cu_9S_5 in Cu_9S_5/PVDFMs from 1 mg to 8 mg improved the amount of water evaporated by the film, however, excess added amount of Cu_9S_5 nanonets (e.g. 12 mg) may block the microporous channels of Cu_9S_5/PVDFM and inhibit the water transport and the release of water vapor, leading to a decrease of the amount of water evaporated. Therefore, the 8 mg-Cu_9S_5/PVDFM showed the maximum water evaporation weight, which was 2.8 and 3.6 times higher than that by pure PVDFM under 1 sun and pure water under 1 sun, respectively.

To evaluate the water evaporation performance, the water evaporation rates (v) were calculated as the following equation (1)[17,34,35]

$$v = \frac{m_{loss}}{\pi\left(\frac{D}{2}\right)^2 t} \qquad (1)$$

where m_{loss} stands for the weight losses of the device due to water evaporation, D is the diameter of as-prepared interfacial evaporator, and t reprensents the irradiation time of each water evaporation experiment. Likewise, to eliminate the effect of natural water evaporation, the evaporation rate of

pure water under dark environment was substracted from all the solar-irradiation water evaporation rates. Figure 3B represented the average water evaporation rates, which followed this order: 1 mg-Cu_9S_5/PVDFM < 2 mg-Cu_9S_5/PVDFM < 4 mg-Cu_9S_5/PVDFM < 12 mg-Cu_9S_5/PVDFM < 8 mg-Cu_9S_5/PVDFM, with the corresponding water evaporation rates of 0.550, 0.793, 1.053, 1.159, and 1.173 kg m^{-2} h^{-1}, respectively. Obviously, the highest water evaporation rate was obtained with the 8 mg-Cu_9S_5/PVDFM.

To further investigate the solar vapor generation performance of Cu_9S_5/PVDFM, the water evaporation tests were studied under various solar intensities (i.e., from 1 sun to 4 sun). As shown in Figure 3C, the average weight of the water evaporated were 0.586, 1.264 and 2.640 kg m^{-2} under 1, 2 and 4 sun, respectively, by the 8 mg-Cu_9S_5/PVDFM. Obviously, the water evaporation weights increased with the increased light intensity irradiation, so did the water evaporation rates (see Figure 3D). As shown, the average water evaporation rates were 1.173, 2.527 and 5.280 kg m^{-2} h^{-1} under 1, 2, and 4 sun, respectively. Also, the solar evaporation rate of 5.280 kg m^{-2} h^{-1} under 4 sun was 12.5 and 16.1 times higher than that of pure PVDFM under 1 sun and pure water under 1 sun, respectively. This indicated an outstanding solar evaporation performance of the Cu_9S_5/PVDFM. To evaluate the reusability and durability of Cu_9S_5/PVDFM, the water evaporation tests of 8 mg-Cu_9S_5/PVDFM were performed recurrently for 20 times under different light densities irradiation. As showed in Figure 2E, the corresponding water evaporation rates were closed to 1.173, 2.527 and 5.280 kg m^{-2} h^{-1} under 1, 2 and 4 sun, respectively, indicating a stable performance of solar vapor generation of Cu_9S_5/PVDFM.

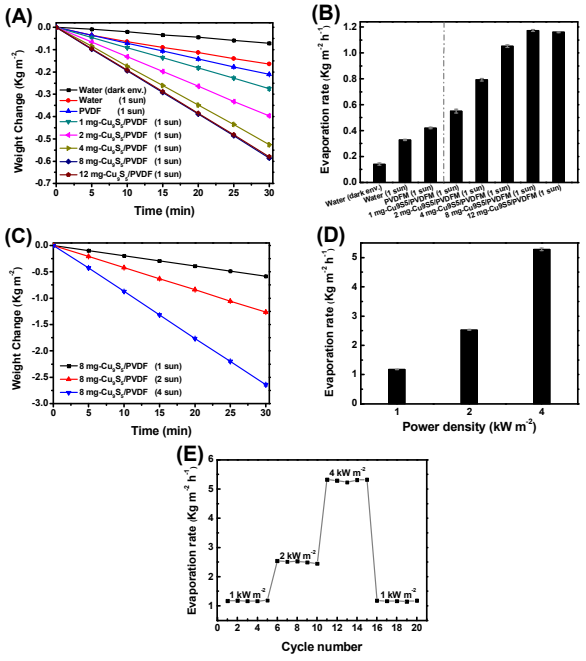

Figure 3. As-prepared samples for solar vapor generation. Weight changes (A) and evaporation rates (B) of pure water under dark environment, pure water under 1 sun, pure water covered with pure PVDFM and pure water covered with Cu_9S_5/PVDFMs with different contents of Cu_9S_5 under 1 sun; The weight changes (C) and evaporation rates (D) of pure water covered with 8 mg-Cu_9S_5/PVDFM under 1, 2 and 4 sun, respectively. All above data are showed as the mean with error bars. (E) The solar vapor generation cycle performance of 8 mg-Cu_9S_5/PVDFM under 1, 2 and 4 sun, respectively.

The IR photos of interfacial evaporators were further used to determine the surface temperatures of the evaporator under different intensities solar irradiation. The initial temperature of pure water was about 25 °C for each solar vapor generation test. Figure 4A-F showed the IR photos of the temperatures after 30 min for pure water under dark environment, pure water under 1 sun, pure water covered with pure PVDFM under 1 sun, and pure water covered with as-prepared 8 mg-Cu_9S_5/PVDFM under 1, 2 and 4 sun irradiation, respectively. Accordingly, the surface temperatures were about 24.9, 30.7, 32.2, 36.1, 45.2 and 54.3 °C, after the corresponding solar vapor generation tests, as shown in the plot of temperatures change of Figure 4G. As shown in Figure 4H, the vapor generated was clearly observed under 4 sun.

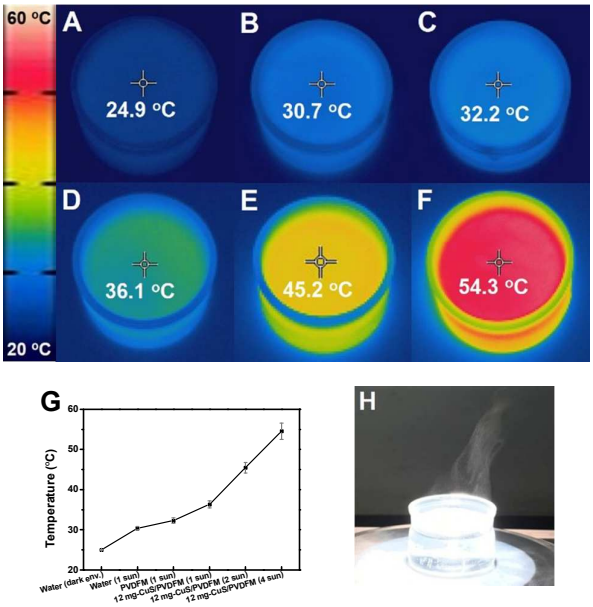

Figure 4. IR photos of pure water under dark environment (A), pure water under 1 sun (B), pure water covered with pure PVDFM (C), and pure water covered with 8 mg-Cu_9S_5/PVDFM under 1, 2 and 4 sun (D-F), respectively; (G) the plot of their surface temperatures change; (H) the photo of vapor generated under 4 sun irradiation.

As well known, another important parameter to evaluate the solar vapor generation performance is solar vapor generation efficiency (η), calculated based on the following equation (2)[46,48]

$$\eta = v \cdot \frac{C \times \Delta T + \Delta_{vap} H_m}{C_{opt} q_i} \qquad (2)$$

Table 2. Efficiency of different samples under different optical concentrations.

C_{opt}	Sample	v (kg m^{-2} h^{-1})	ΔT (°C)	CΔT (kJ kg^{-1})	$\Delta_{vap}H_m$(kJ kg^{-1})	η (%)
1	Pure water	0.328±0.006	5.6±0.5	23.41±2.09	2427	22.2±0.4
1	PVDFM	0.421±0.007	7.3±0.7	30.51±2.93	2424	28.7±0.5
1	8 mg-Cu_9S_5/PVDFM	1.173±0.007	11.4±0.9	47.65±3.76	2415	80.2±0.6
2	8 mg-Cu_9S_5/PVDFM	2.527±0.010	20.6±1.3	86.11±5.43	2393	87.0±0.7
4	8 mg-Cu_9S_5/PVDFM	5.280±0.050	29.6±2.1	123.73±8.78	2371	91.5±1.1

Table 3. Comparison of solar vapor generation performance of various interfacial plasmonic evaporators.

Interfacial plasmonic evaporators	Classification of light-harvesting materials	Light sources	Power density (kW·m^{-2})	Efficiency	Ref.
Au/Al_2O_3 composite	Plasmonic-metal	Solar simulator	1	~49%*	23
Al/Al_2O_3 composite	Plasmonic-metal	Solar simulator	1	~57.5%	29
Au/filter paper composite	Plasmonic-metal	Solar simulator	1	~62.5%*	25
Pd/wood composite	Plasmonic-metal	Solar simulator	1	~69%	30
Au/PBO nanofiber composite	Plasmonic-metal	Solar simulator	1	83%	26
Paper-based AuNP film	Plasmonic-metal	Solar simulator	4.5	~77.8%*	24
Black Au membrane	Plasmonic-metal	Solar simulator	20	~57%	21
Au aerogel	Plasmonic-metal	808 nm laser	51	76.3%*	22
TiN/microfiber composite	Plasmonic-ceramic	Solar simulator	1	>80%*	31
Ti_3C_2/PVDFM	Plasmonic-ceramic	Solar simulator	1	84%*	32
Ti_3C_2/MCE membrane	Plasmonic-ceramic	Solar simulator	1	71%	33
$W_{18}O_{49}$/PTFE membrane	Plasmonic-semiconductor	Solar simulator	1	80.7%*	41
Cu_7S_4 nanocrystals film	Plasmonic-semiconductor	Infrared lamp	1	~77.1%	38
CuS/PE membrane	Plasmonic-semiconductor	Solar simulator	1	~63.9%*	63
CuS/SCM	Plasmonic-semiconductor	Solar simulator	1	~68.6%*	34
Cu_9S_5/MCE membrane	Plasmonic-semiconductor	Solar simulator	1	~60.1%*	13
CuS/MCE membrane	Plasmonic-semiconductor	Solar simulator	1	80±2.5%*	13
CdS-Cu_7S_4 film	Plasmonic-semiconductor	Solar simulator	1.5	~48.4%*	35
Cu_9S_5/PVDFM	Plasmonic-semiconductor	Solar simulator	1	80.2±0.6%	This work

The symbol "*" refers to the data without subtracting natural water evaportion in their works.

where v denotes the evaporation rate, c represents the specific heat capacity of water (4.18 J g^{-1} K^{-1}), ΔT is the temperature variation from the initial temperature (~24.9 °C) of water to final vapor temperature, and $\Delta_{vap}H_m$ is the liquid-vapor phase change enthalpy, C_{opt} is the optical concentration and q_i is the incident solar irradiation density of 1 kW·m^{-2}. Table 2 showed the detail parameters of the solar vapor generation tests with different samples under different optical concentrations. As calculated by the obove equation (2), the water evaporation efficiencies of 8 mg-Cu_9S_5/PVDFM were about 80.2, 87.0 and 91.5% under 1, 2 and 4 sun, respectively. For comparison, the water evaporation efficiencies were only about 22.2 and 28.7% for pure water and pure water covered by pure PVDFM, respectively. As showed, the water evaporation efficiencies increased with the increased optical concentrations from 1 sun to 4 sun, further increase of solar intensity may lead to more high efficiency. However, considering the practical application for solar vapor generation is irradiated outdoor under the solar intensity of ~1 kW/m^{-2}, ever-increasing the solar intensity is unnecessary. Interestingly, the water evaporation efficiencies of 91.5±1.1% under 4 sun were very close to the value of solar absorptance of ~91.7%. This might be attributed to the temperature of the bulk water beneath the air-water interface increased sharply under the higher simulated sunlight irradiation (e.g., 4 sun), as found in the IR photo of Figure 4F. So the higher temperature of the bulk water beneath the air-water interface could accelerate the water evaporation. Moreover, the high bulk water temperature may cause some water bubble to transpire into air directly without the phase transition from liquid to vapor.[26] So it is possible for the absorbers that the solar vapor efficiencies are close to or higher than value of solar absorptance.[66-67]

In Table 3, we compared part of the water evaporation efficiencies of the recent reports using different interfacial plasmonic evaporators (e.g., plasmonic-metals-based,[21-26,29,30] plasmonic-ceramics-based,[31-33] plasmonic-semiconductors-based[13,34,35,38,41,63]). Here, it is noteworthy that the values of efficiency labelled by the asterisk are inaccurate due to neglecting the effect of natural water evaporation. To our knowledge, the effect of natural water evaporation is considerable and should be subtracted while calculating the water evaporation efficiency under solar irradiation. We estimate that the data could decrease ca. 10%. For instance, in this work, the efficiency of water evaporation of 8 mg-Cu_9S_5/PVDFM is ~80.2% under 1 sun, however, the corresponding evaporation efficiency is ~90% if the evaporation rate of pure water under dark environment was not subtracted. In view of this, the water evaporation efficiency of our Cu_9S_5/PVDFM of ~80.2% under 1 sun irradiation is top-ranking in the three plasmonic evaporators reported so far. Furthermore, with the advantages of the

straightforward fabrication process, the inexpensive materials, and the excellent reusability, the Cu_9S_5/PVDFM had demonstrated its strong competitiveness over others for solar vapor applications.

Conclusions

In summary, we have demonstrated a Cu_9S_5/PVDFM with integrative porous membrane structure, for solar vapor generation. The Cu_9S_5/PVDFM exhibits a large solar absorptance of ~91.7% in the 250-2000 nm wavelength region, and enables the water evaporation efficiencies to reach 80.2±0.6% and 91.5±1.1% under the solar irradiation intensities of 1 sun and 4 sun, respectively. It has been reused over 20 times without performance degradation, exhibiting an excellent reusability and durability. With simple preparation technology, low-cost feature and high water evaporation efficiency, the Cu_9S_5/PVDFM composite shows a great potential for solar vapor generation, and likely for other applications as well, such as water purification, sterilization, distillation, and desalination.

Experimental

Materials

N, N-Dimethylformamide (DMF) was purchased from Shanghai Sinopharm Chemical Reagent Co. Ltd. Poly (vinylidene fluoride) (PVDF) was purchased from Shandong Xiya Reagent Co. Ltd. The deionized water was purified by a Milli-Q system (Millipore).

Preparation of Cu_9S_5/PVDF membrane

The preparation and characterization of Cu_9S_5 nanonets were based on the report in our previous work.[36] Specifically, the Cu_9S_5 obtained at reaction time of 18 h was chosen as the photothermal conversion material. The Cu_9S_5/PVDFMs were prepared as follows.[10,27,65] Firstly, 2 g PVDF powder was added into 30 mL DMF solution and stirred to get a PVDF/DMF solution. Then, 116 mg Cu_9S_5 was added into a 10 mL beaker containing 1 mL PVDF/DMF solution to form a Cu_9S_5/PVDF/DMF mixture solution under sonication. The Cu_9S_5/PVDF/DMF solution was transferred with a 3 mL pipette to a flat glass surface, and casted by a 150 um gap scraper to form the Cu_9S_5/PVDFM composite. The flat glass coated with Cu_9S_5/PVDFM was immersed in a deionized water bath for 0.5 h and the Cu_9S_5/PVDFM film was off from the flat glass, washed with ethanol several times and dried in a vacuum oven at 45 ^{o}C for 1.5 h. Finally, the Cu_9S_5/PVDFM was trimmed into a round disk shape with a diameter of 33.5 mm. Hence, the Cu_9S_5/PVDFM with 8 mg Cu_9S_5 nanonets added (i.e., 8 mg-Cu_9S_5/PVDFM) was fabricated. The same method was used to prepare other samples with various amount of Cu_9S_5 light absorber, e.g., 1 mg-Cu_9S_5/PVDFM, 2 mg-Cu_9S_5/PVDFM, 4 mg-Cu_9S_5/PVDFM, 12 mg-Cu_9S_5/PVDFM, and pure PVDFM (i.e., without any Cu_9S_5 nanonets added).

Characterization

The morphology and structure were analyzed with field-emission scanning electron microscope (JSM-6700F, Japan) and Leica microscope (DM500, Germany). The contact angle was measured with a contact-angle analyzer (JC2000D1, China). The UV-vis-NIR transmittance and diffuse reflectance spectra were measured on a Lambda 950 UV-vis-NIR scanning spectrophotometer (PerkinElmer, America). The IR digital pictures were captured with an FLIR camera (E40, America).

Solar vapor generation

The solar vapor generation tests were conducted under a homemade chamber optical measurement system, with a PLS-SXE300/300UV solar simulator and other optical components (Perfect Light Technology Co. Ltd, Beijing). The optical irradiation intensities from 1 to 4 sun ($kW{\cdot}m^{-2}$) were measured by an optical power meter (VLP-2000, China). The Cu_9S_5/PVDFM was placed in a 40 mm × 25 mm weighing bottle containing 20 mL deionized water as the solar vapor generation setup. Here, it is important to note that due to the difference of hydrophilic-hydrophobic property of the upper and bottom sides of the Cu_9S_5/PVDFM, the hydrophilic surface (called bottom side) of the Cu_9S_5/PVDFM was placed face down that can contact with bulk water directly, so the hydrophobic surface (called upper side) was placed upward. The weight change during solar vapor generation was recorded using a 4 decimal electronic precision balance (OHRUS FR224CN, accurary: 0.1 mg). For cycling water evaporation tests, after each cycle, the wetted Cu_9S_5/PVDFM was dried under ambient conditions to simulate the actual usage.

Conflicts of interest

There are no conflicts to declare.

Acknowledgements

X. C. is thankful for the support from the U.S. National Science Foundation (DMR-1609061). Y. Z. and X. C. thank the support from the National Key R & D Program of China (no. 2016YFB0300704). Y. Y. acknowledges the State Key Development Program forBasic Research of China (no. 2014CB643306). X. C. appreciates the NSF of Shanghai (no. 17ZR1440900). Y. L. acknowledges the National Nature Science Foundation of China (no. 51602195). F. T. thanks the support from the Doctoral Innovation Foundation ofSMU (no. 2016ycx037), and the Doctoral Excellent Thesis Project Fundation of SMU (no. 2017BXLP005).

Author contributions

F. Tao, K. Yin, and S. Cao prepared the samples. X. Chang, Y. Lei and D. Wang characterized the samples. F. Tao, K. Yin, S. Cao, D. Wang performed the solar vapor generation tests. F. Tao wrote this manuscript. R. Fan, L. Dong, and Y. Yin discussed

and critically read the manuscript. Y. Zhang and X. Chen designed this project and polished this manuscript.

Notes and references

1 Z. Wang, C. Yang, T. Lin, H. Yin, P. Chen, D. Wan, F. Xu, F. Huang, J. Lin, X. Xie, M. Jiang, *Energy Environ. Sci.*, 2013, **6**, 3007-3014.
2 T. Lin, C. Yang, Z. Wang, H. Yin, X. Lü, F. Huang, J. Lin, X. Xie, M. Jiang, *Energy Environ. Sci.*, 2014, **7**, 967-972.
3 Z. Wang, C. Yang, T. Lin, H. Yin, P. Chen, D. Wan, F. Xu, F. Huang, J. Lin, X. Xie, M. Jiang, *Adv. Funct. Mater.*, 2013, **23**, 5444-5450.
4 X. Chen, L. Liu, P. Yu, S. Mao, *Science*, 2011, **331**, 746-750.
5 V. Zardetto, B. Williams, A. Perrotta, F. Giacomo, M. Verheijen, R. Andriessen, W. Kessels, M. Creatore, *Sustainable energy fuels*, 2017, **1**, 30-55.
6 G. Ni, G. Li, S. Boriskina, H. Li, W. Yang, T. Zhang, G. Chen, *Nat. Energy*, 2016, **1**, 16126.
7 M. Elimelech, *J. Water Supply Res. Technol. AQUA*, 2006, **55**, 3-10.
8 M. Mekonnen, A. Hoekstra, *Sci. Adv.*, 2016, **2**, e1500323.
9 W. Shang, T. Deng, *Nat. Energy*, 2016, **1**, 16133.
10 L. Yi, S. Ci, S. Luo, P. Shao, Y. Hou, Z. Wen, *Nano Energy*, 2017, **41**, 600-608.
11 V. Kashyap, A. Al-Bayati, S. Sajadi, P. Irajizad, S. Wang, H. Ghasemi, *J. Mater. Chem. A*, 2017, **5**, 15227-15234.
12 G. Wang, Y. Fu, X. Ma, W. Pi, D. Liu, X. Wang, *Carbon*, 2017, **114**, 117-124.
13 Z. Guo, X. Ming, G. Wang, B. Hou, X. Liu, T. Mei, J. Li, J. Wang, X. Wang, *Semicond. Sci. Technol.*, 2018, **33**, 025008.
14 Y. Li, T. Gao, Z. Yang, C. Chen, W. Luo, J. Song, E. Hitz, C. Jia, Y. Zhou, B. Liu, B. Yang, L. Hu, *Adv. Mater.*, 2017, **29**, 1700981.
15 H. Ghasemi, G. Ni, A. Marconnet, J. Loomis, S. Yerci, N. Miljkovic, G. Chen, *Nat. Commun.*, 2014, **5**, 4449.
16 Y. Wang, L. Zhang, P. Wang, *ACS Sustainable Chem. Eng.*, 2016, **4**, 1223-1230.
17 F. Tao, Y. Zhang, B. Wang, F. Zhang, X. Chang, Y. An, R. Fan, L. Dong, Y. Yin, *Sol. Energy Mat. Sol. Cells*, 2018, **180**, 34-45.
18 P. Zhang, J. Li, L. Lv, Y. Zhao, L. Qu, *ACS Nano*, 2017, **11**, 5087-5093.
19 X. Li, W. Xu, M. Tang, L. Zhou, B. Zhu, S. Zhu, J. Zhu, *PNAS*, 2016, **113**, 13953-13958.
20 L. Shi, Y. Wang, L. Zhang, P. Wang, *J. Mater. Chem. A*, 2017, **5**, 16212-16219.
21 K. Bae, G. Kang, S. Cho, W. Park, K. Kim, W. Padilla, *Nat. Commun.*, 2015, **6**, 10103.
22 L. Tian, J. Luan, K. Liu, Q. Jiang, S. Tadepalli, M. Gupta, R. Naik, S. Singamaneni, *Nano Lett.*, 2016, **16**, 609-616.
23 L. Zhou, S. Zhuang, C. He, Y. Tan, Z. Wang, J. Zhu, *Nano Energy*, 2017, **32**, 195-200.
24 Y. Liu, S. Yu, R. Feng, A. Bernard, Y. Liu, Y. Zhang, H. Duan, W. Shang, P. Tao, C. Song, T. Deng, *Adv. Mater.*, 2015, **27**, 2768-2774.
25 X. Wang, Y. He, X. Liu, G. Cheng, J. Zhu, *Appl. Energy*, 2017, **195**, 414-425.
26 M. Chen, Y. Wu, W. Song, Y. Mo, X. Lin, Q. He, B. Guo, *Nanoscale*, 2018, **10**, 6186-6193.
27 A. Politano, P. Argurio, G. Profio, V. Sanna, A. Cupolillo, S. Chakraborty, H. Arafat, E. Curcio, *Adv. Mater.*, 2017, **29**, 1603504.
28 H. Wang, L. Miao, S. Tanemura, *Sol. RRL*, 2017, **1**,1600023.
29 L. Zhou, Y. Tan, J. Wang, W. Xu, Y. Yuan, W. Cai, S. Zhu, J. Zhu, *Nat. Photonics*, 2016, **10**, 393-398.
30 M. Zhu, Y. Li, F. Chen, X. Zhu, J. Dai, Y. Li, Z. Yang, X. Yan, J. Song, Y. Wang, E. Hitz, W. Luo, M. Lu, B. Yang, L. Hu, *Adv. Energy Mater.*, 2017, **8**, 1701028
31 M. Kaur, S. Ishii, S. Shinde, T. Nagao, *ACS Sustainable Chem. Eng.*, 2017, **5**, 8523-8528.
32 R. Li, L. Zhang, L. Shi, P. Wang, *ACS Nano*, 2017, **11**, 3752-3759.
33 J. Zhao, Y. Yang, C. Yang, Y. Tian, Y. Han, J. Liu, X. Yin, W. Que, *J. Mater. Chem. A*, 2018, **6**, 16196-16204.
34 F. Tao, Y. Zhang, S. Cao, K. Yin, X. Chang, Y. Lei, R. Fan, L. Dong, Y. Yin, X. Chen, *Mater. Today Energy*, 2018, **9**, 285-294.
35 F. Tao, Y. Zhang, F. Zhang, K. Wang, X. Chang, Y. An, L. Dong, Y. Yin, *ChemistrySelect*, 2017, **2**, 3039-3048.
36 F. Tao, Y. Zhang, F. Zhang, Y. An, L. Dong, Y. Yin, *RSC Adv.*, 2016, **6**, 63820-63826.
37 F. Tao, Y. Zhang, F. Zhang, L. Yang, Y. An, Y. Yin, *Mater. Lett.*, 2015, **140**, 166-169.
38 C. Zhang, C. Yan, Z. Xue, W. Yu, Y. Xie, T. Wang, *Small*, 2016, **12**, 5320-5328.
39 S. Zhang, C. Sun, J. Zeng, Q. Sun, G. Wang, Y. Wang, Y. Wu, D. Dou, M. Gao, Z. Li, *Adv. Mater.*, 2016, **28**, 8927-8936.
40 A. Poulose, S. Veeranarayanan, M. Mohamed, R. Aburto, T. Mitcham, R. Bouchard, P. Ajayan, Y. Sakamoto, T. Maekawa, D. Kumar, *Sci. Rep.*, 2016, **6**, 35961.
41 Y. Chang, Z. Wang, Y. Shi, X. Ma, L. Ma, Y. Zhang, J. Zhan, *J. Mater. Chem. A*, 2018, **6**, 10939-10946.
42 Z. Chen, Q. Wang, H. Wang, L. Zhang, G. Song, L. Song, J. Hu, H. Wang, J. Liu, M. Zhu, D. Zhao, *Adv. Mater.*,2013, **25**, 2095-2100.
43 T. Chala, C.Wu, M. Chou, M. Gebeyehu, K. Cheng, *Nanomaterials*, 2017, **7**, 191.
44 J. Wang, Y. Li, L. Deng, N. Wei, Y. Weng, S. Dong, D. Qi, J. Qiu, X. Chen, T. Wu, *Adv. Mater.*, 2017, **29**, 1603730.
45 X. Yang, Y. Yang, L. Fu, M. Zou, Z. Li, A. Cao, Q. Yuan, *Adv. Funct. Mater.*, 2018, **28**, 1704505.
46 Z. Guo, G. Wang, X. Ming, T. Mei, J. Wang, J. Li, J. Qian, X. Wang, *ACS Appl. Mater. Interfaces*, 2018, **10**, 24593-24589.
47 N. Xu, X. Hu, W. Xu, X. Li, L. Zhou, S. Zhu, J. Zhu, *Adv. Mater.*, 2017, **29**, 1606762.
48 Z. Deng, P. Liu, J. Zhou, L. Miao, Y. Peng, H. Su, P. Wang, X. Wang, W. Cao, F. Jiang, L. Sun, S. Tanemura, *Sol. RRL*, **2018**, 1800073.
49 P. Liu, L. Miao, Z. Deng, J. Zhou, H. Su, L. Sun, S. Tanemura, W. Cao, F. Jiang, L. Zhao, *Mater. Today Energy*, 2018, **8**, 166-173.
50 K. Kim, S. Yu, C. An, S. Kim, J. Jang, *ACS Appl. Mater. Interfaces*, 2018, **10**, 15602-15608.
51 F. Zhao, X. Zhou, Y. Shi, X. Qian, M. Alexander, X. Zhao, S. Mendez, R. Yang, L. Qu, G. Yu, *Nat. Nanotechnol.*, 2018, **13**, 489-495.
52 J. Song, C. Chen, Z. Yang, Y. Kuang, T. Li, Y. Li, H. Huang, I. Kierzewski, B. Liu, S. He, T. Gao, S. Yuruker, A. Gong, B. Yang, L. Hu, *ACS Nano*, 2018, **12**, 140-147.
53 X. Yin, Y. Zhang, Q. Guo, X. Cai, J. Xiao, Z. Ding, J. Yang, *ACS Appl. Mater. Interfaces*, 2018, **10**, 10998-11007.
54 Y. Liu, J. Chen, D. Guo, M. Cao, L. Jiang, *ACS Appl. Mater. Interfaces*, 2015, **7**, 13645-13652.
55 Q. Liu, Y. Liu, Y. Yin, *Natl. Sci. Rev.*, 2018, **5**, 128-130.
56 L. Zhu, M. Gao, C. Peh, G. Ho, *Mater. Horiz.*, 2018, **5**, 323-343.
57 M. Sigman, A. Ghezelbash, T. Hanrath, A. Saunders, F. Lee, B. Korgel, *J. Am. Chem. Soc.*, 2003, **125**, 16050-16057.
58 N. Morimoto, *Mineral. J.*, 1962, **3**, 338-344.
59 J. Park, S. Kim, J. Chang, H. Seo, J. Lee, J. Yuk, *Nat. Commun.*, 2018, **9**, 922.
60 Y. Hsu, Y. Chen, Y. Lin, *Electrochim. Acta*, 2014, **139**, 401-407.

61 C. Tan, Y. Zhu, R. Lu, P. Xue, C. Bao, X. Liu, Z. Fei, Y. Zhao, *Mater. Chem. Phys.*, 2005, **91**, 44-47.
62 Q. Lu, F. Gao, D. Zhao, *Nano Lett.*, 2002, **2**, 725-728.
63 M. Shang, N. Li, S. Zhang, T. Zhao, C. Zhang, C. Liu, H. Li, Z. Wang, *ACS Appl. Energy Mater.*, 2018, **1**, 56-61.
64 Y. Wang, C. Wang, X. Song, M. Huang, S. Megarajan, S. Shaukat, H. Jiang, *J. Mater. Chem. A*, 2018, **6**, 9874-9881.
65 E. Fontananova, J. Jansen, A. Cristiano, E. Curcio, E. Drioli, *Desalination*, 2006, **192**,190-197.
66 X. Wu, G. Chen, W. Zhang, X. Liu, H. Xu, *Adv. Sustainable Syst.*, 2017, **1**, 1700046.
67 L. Zhang, J. Xing, X. Wen, J. Chai, S. Wang, Q. Xiong, *Nanoscale*, 2017, **9**, 12843-12849.

Graphic Abstract

A novel plasmonic interfacial evaporator composed of Cu_9S_5 nanonets and PVDFM has shown high efficiencies of 80.2±0.6% and 91.5±1.1% under 1 and 4 sun irradiation, respectively, for solar vapor generation.